Proceedings of the Project Review, Geo-Mathematical Imaging Group (Purdue University, West Lafayette IN), Vol. 1 (2009) pp. 133-156.

KINEMATICS OF SHOT-GEOPHONE MIGRATION AND RIEMANNIAN ANNIHILATORS

CHRISTIAAN C. STOLK *, MAARTEN V. DE HOOP †, AND WILLIAM W. SYMES ‡

Abstract. Recent analysis and synthetic examples have shown that many prestack depth migration methods produce non-flat image gathers containing spurious events, even when provided with a kinematically correct migration velocity field, if this velocity field is highly refractive. This pathology occurs in all migration methods which produce partial images as independent migrations of data bins. *Shot-geophone prestack depth migration* is an exception to this pattern: each point in the prestack image volume depends explicitly on all traces within the migration aperture. We use a ray-theoretical analysis to show that shot-geophone migration produces focussed (subsurface offset domain) or flat (scattering angle domain) image gathers, regardless of velocity field complexity, provided that there is a curvilinear coordinate system defining pseudodepth with respect to which the rays carrying significant energy do not turn, and that the acquisition coverage is sufficient to determine all such rays. While our analysis is theoretical and idealized, we present a synthetic example which suggests that its implications remain valid for practical implementations, and that shot-geophone prestack depth migration may be a particularly appropriate tool for velocity analysis in complex structure.

1. Introduction. The basis of migration velocity analysis is the *semblance principle*: prestack migrated data volumes contain *flat image gathers*, i.e. are at least kinematically independent of the bin or stacking parameter, when the velocity is correct [18, 38]. Migration velocity analysis (as opposed to standard NMO-based velocity analysis) is most urgently needed in areas of strong lateral velocity variation, i.e. "complex" structure such as salt flanks, chalk tectonics, and overthrust geology. However strong refraction implies multiple raypaths connecting source and receiver locations with reflection points, and multiple raypaths in turn imply that the semblance principle is not valid: that is, image gathers are *not* in general flat, even when the migration velocity closely approximates the true propagation velocity [33].

The failure of the semblance principle in complex structure afflicts all prestack migration techniques in which each data bin creates an independent (partial) image of the subsurface. This category includes many variants of common shot, common offset and common scattering angle migration [20, 21, 37, 7, 34, 33]. Note that gathers fail to be flat for numerous reasons other than that explained in [33] - the causes include finite migration aperture and data frequency content, numerical inaccuracies in traveltime computation or wavefield extrapolation, and (of course) inaccurate migration velocity. The result in [33] shows that, even if *all* of these other sources of error are corrected, a geometrical obstruction to flat gathers remains. Since these kinematic artifacts interfere destructively ("stack out") in the final image formation, their presence is mostly an issue for velocity analysis (and possibly for inference of elastic parameters). As shown for example in [21], in image gathers produced with inaccurate velocities, the artifacts are indistinquishable from the actual events and thus can obstruct successful velocity updating.

However one well-known form of prestack image formation does *not* form partial images as *independent* prestack migrations of data bins: this is Claerbout's *survey-sinking migration* [8, 9]. This migration method is commonly implemented using an approximate one-way wave equation to extrapolate the source and receiver wavefields. Such depth extrapolation implementation presumes that rays carrying significant energy do not turn horizontal. Source and receiver wavefields may be extrapolated separately, and correlated at each depth ("shot profile" or "shot record" migration), or extrapolated simultaneously ("DSR" migration): in principle, the two produce equivalent image volumes [30, 4, 31, 32]. In either case, the prestack migration output at each image point depends on a range of sources and receivers, not on data from a single bin defined by fixing any combination

*Korteweg-de Vries Institute for Mathematics, Plantage Muidergracht 24, 1018 TV Amsterdam, The Netherlands, email c.c.stolk@uva.nl

†Center for Computational and Applied Mathematics and Geo-Mathematical Imaging Group, Purdue University, West Lafayette, IN 47907, USA, email mdehoop@purdue.edu

‡The Rice Inversion Project, Department of Computational and Applied Mathematics, Rice University, Houston TX 77251-1892 USA, email symes@caam.rice.edu

of acquisition parameters.

This paper analyzes the kinematics of an idealized version of Claerbout's migration method. We shall call it, for want of a better name, *shot-geophone migration*. We emphasize that this term, as used in this paper, does not imply any particular method of wavefield extrapolation, or a choice between separate or simultaneous extrapolation of source and receiver wavefields. Our idealized shot-geophone migration encompasses both shot profile and DSR migration methods; all practical realizations of these can be viewed as approximations of our idealized method. In fact, even depth extrapolation (one-way wave propagation) is not intrinsic to the definition of this idealized migration operator. Both two-way reverse time and Kirchhoff (diffraction sum) realizations are possible, and inherit the same theoretical properties.

Our analysis demonstrates that a semblance principle appropriate for shot-geophone migration holds (at least theoretically) *regardless of velocity field complexity*, assuming

- there is a curvilinear coordinate system defining pseudodepth with respect to which the rays carrying significant energy do not turn;
- the survey contains enough data to determine wavefield kinematics (for example, areal or "true 3D" acquisition in general, or narrow azimuth data plus mild cross-line heterogeneity); and
- the migration velocity field is kinematically correct

In the flat coordinate system, this result was established by Stolk and De Hoop [30]. We give a somewhat simpler derivation of this property.

The semblance principle appropriate for shot-geophone migration takes several roughly equivalent forms, corresponding to several available methods for forming image gathers. Sherwood and Schultz [27], Claerbout [9], and others defined image gathers depending on (subsurface) offset and depth: in such *offset image gathers*, energy is *focussed* at zero offset when the velocity is kinematically correct. De Bruin et al. [10] and Prucha et al [22] gave one definition of *angle image gathers*, while Sava and Fomel [25] suggest another. Such gathers are functions of scattering angle and depth. In both cases, correct migration velocity focusses energy at *zero slope*, i.e. angle image gathers are flattened at correct migration velocity. In consequence, angle imaging via shot-geophone migration, using either method of angle gather formation mentioned above, is *not* equivalent, even kinematically, to Kirchhoff common angle imaging [37, 7] - indeed, the latter typically generates kinematic artifacts when multiple ray paths carry important energy.

Theoretical properties are interesting only insofar as they have observable practical effect. We present a synthetic example in which the prestack image volume has the properties predicted by the theory. We chose an example for which prior analysis had already shown the existence of kinematic artifacts in common offset or common scattering angle Kirchhoff migration. We used a shot-geophone migration based on solving Helmholtz equations [29]. Apart from any implementation defects or limitations of the data, image amplitudes may have only an indirect relation to reflection strength, and may disappear altogether in shadow zones. However, where image energy is present, it will be focused (offset image gathers) or appear in flat events (angle image gathers), with no apparent kinematics artifacts. The apparent fidelity of the examples to the theory also supports our contention that the theoretical predictions of our analysis survive implementation imperfections.

The semblance principle is a result of the mathematical structure of shot-geophone migration, not of any particular approach to its implementation. Migration operators are dual or *adjoint* to modeling operators. The various prestack migration operators are adjoint to *extended Born modeling* operators, and differ in the way in which Born modeling is extended. The ray geometry of these extended modeling operators is the crux of our analysis. The semblance principle and imaging condition of each prestack migration operator are inherent in the definition of the corresponding extended Born model, which in some sense "explains" these concepts.

The "enough data" condition listed second above is quite as important as the others, as will be explained below. For arbitrary 3D complexity in the migration velocity field, validity of the semblance principle requires areal coverage ("true 3D" data). In particular we cannot guarantee the absence of kinematic artifacts in shot-geophone migration of narrow azimuth data, unless the

velocity model is assumed to have additional properties, for example mild cross-line heterogeneity, which compensate to some extent for the lack of azimuths. This issue will be discussed a bit more in the concluding section.

Sherwood and Schultz [27] observed that the focussing property of shot-geophone migration might serve as the basis for an approach to velocity estimation. Its freedom from artifacts suggests that shot-geophone migration may be a particularly appropriate tool for migration velocity analysis of data acquired over complex structures. Some investigations of this idea have been carried out by [28, 24, 13, 2].

The paper begins with a description of the idealized shot-geophone migration operator as adjoint to an *extended* Born (single-scattering) modeling operator. All prestack migration methods, including those based on data binning, can be described in this way, as adjoint to extended modeling of some sort. The basic kinematics of shot-geophone prestack migration then follow easily from the high-frequency asymptotics of wave propagation. We summarize these kinematic properties, and present the outline of a complete derivation in the Appendix. The artifact-free result of Stolk and De Hoop [30] follows easily from the general kinematic properties already described, for both offset image gathers and angle image gathers in the style of Sava and Fomel [25]. We also review an alternative construction of angle image gathers due to De Bruin et al. [10]. We show how the semblance property for this form of angle domain migration follows from the general properties of shot-geophone migration.

Finally we present an example illustrating the semblance property, using 2D synthetic data of significant ray path complexity. The example contrasts the angle image gathers produced by (Kirchhoff or Generalized Radon Transform) common scattering angle migration [11, 37, 7] with those produced by shot-geophone migration. Kinematic artifacts appear *and can be unambiguously identified as kinematic artifacts* in the former, but do not appear in the latter.

2. Shot-geophone migration as adjoint of extended Born modeling. We assume that sources and receivers lie on the same depth plane, and adjust the depth axis so that the source-receiver plane is $z = 0$. This restriction can be removed at the cost of more complicated notation (and numerics): it is not essential. Nothing about the formulation of the migration method presented below *requires* that data be given on the full surface $z = 0$.

While the examples to be presented later are all 2D, the construction is not: in the following $\mathbf{x}$ (and other bold face letters) will denote either two- or three-dimensional vectors. Source locations are $\mathbf{x}_s$, receiver locations are $\mathbf{x}_r$.

2.1. Single scattering. The causal acoustic Green's function $G(\mathbf{x}, t; \mathbf{x}_s)$ for a point source at $\mathbf{x} = \mathbf{x}_s$ is the solution of

$$\frac{1}{v^2(\mathbf{x})}\frac{\partial^2 G}{\partial t^2}(\mathbf{x}, t; \mathbf{x}_s) - \nabla^2_{\mathbf{x}} G(\mathbf{x}, t; \mathbf{x}_s) = \delta(\mathbf{x} - \mathbf{x}_s)\delta(t), \tag{2.1}$$

with $G = 0, t < 0$.

In common with all other migration methods, shot-geophone migration is based on the Born or single scattering approximation. Denote by $r(\mathbf{x}) = \delta v(\mathbf{x})/v(\mathbf{x})$ a relative perturbation of the velocity field. Linearization of the wave equation yields for the corresponding perturbation of the Green's function

$$\frac{1}{v^2(\mathbf{x})}\frac{\partial^2 \delta G}{\partial t^2}(\mathbf{x}, t; \mathbf{x}_s) - \nabla^2_{\mathbf{x}} \delta G(\mathbf{x}, t; \mathbf{x}_s) = \frac{2r(\mathbf{x})}{v^2(\mathbf{x})}\frac{\partial^2}{\partial t^2} G(\mathbf{x}, t; \mathbf{x}_s), \tag{2.2}$$

whose solution has the integral representation at the source and receiver points $\mathbf{x}_r, \mathbf{x}_s$

$$\delta G(\mathbf{x}_r, t; \mathbf{x}_s) = \frac{\partial^2}{\partial t^2} \int d\mathbf{x}\, \frac{2r(\mathbf{x})}{v^2(\mathbf{x})} \int d\tau\, G(\mathbf{x}, t - \tau; \mathbf{x}_r) G(\mathbf{x}, \tau; \mathbf{x}_s). \tag{2.3}$$

The singly scattered field is the time convolution of δG with a source wavelet (or the space-time convolution with a radiation pattern operator, for more complex sources). Since the principal

concern of this paper is kinematic relationships between data and image, we ignore the filtering by the source signature (i.e. replace it with a delta function). This effective replacement of the source by an impulse does not seem to invalidate the predictions of the theory, though the matter is certainly worthy of more study.

The Born modeling operator $F[v]$ is

$$F[v]r(\mathbf{x}_r,t;\mathbf{x}_s)=\delta G(\mathbf{x}_r,t;\mathbf{x}_s). \tag{2.4}$$

2.2. Common Offset Modeling and Migration. Basic versions of all prestack migration operators result from two further modeling steps:

(i) extend the definition of reflectivity to depend on *more spatial degrees of freedom*, inserted somehow into the Born modeling formula (equation 2.2 or 2.3) in such a way that when the extra degrees of freedom are present in some specific way ("physical reflectivity"), Born modeling is recovered;

(ii) form the adjoint of the extended modeling operator: this is a prestack migration operator. The output of the adjoint operator is the prestack image; it depends on the same degrees of freedom as the input of the modeling operator.

Prestack common offset modeling results from replacing $2r(\mathbf{x})/v^2(\mathbf{x})$ with $R(\mathbf{x},\mathbf{h})$, where $\mathbf{h}$ is vector half-offset: $\mathbf{h}=\frac{1}{2}(\mathbf{x}_r-\mathbf{x}_s)$. $\mathbf{x}$ is not necessarily located below the midpoint. Denote by $\mathbf{x}_m=\frac{1}{2}(\mathbf{x}_r+\mathbf{x}_s)$ the corresponding midpoint vector.

The additional degrees of freedom mentioned in (i) above are the components of source-receiver half-offset. This extended reflectivity is inserted into the Born modeling formula to give the extended common offset modeling operator $\bar{F}[v]$:

$$\bar{F}_{\rm co}[v]R(\mathbf{x}_r,t;\mathbf{x}_s)=u(\mathbf{x}_r,t;\mathbf{x}_s), \tag{2.5}$$

where

$$u(\mathbf{x}_m+\mathbf{h},t;\mathbf{x}_m-\mathbf{h})=\frac{\partial^2}{\partial t^2}\int d\mathbf{x}\,R(\mathbf{x},\mathbf{h})\int d\tau\,G(\mathbf{x},t-\tau;\mathbf{x}_m+\mathbf{h})G(\mathbf{x},\tau;\mathbf{x}_m-\mathbf{h}). \tag{2.6}$$

If $R(\mathbf{x},\mathbf{h})=2r(\mathbf{x})/v^2(\mathbf{x})$ is actually independent of $\mathbf{h}$, then the output $u(\mathbf{x}_r,t;\mathbf{x}_s)$ of equation 2.6 is identical to the perturbational Green's function $\delta G(\mathbf{x}_r,t;\mathbf{x}_s)$ as is clear from comparing equations 2.6 and 2.3. That is, the Born forward modeling operator is the "spray" operator ,

$$r(\mathbf{x})\mapsto R(\mathbf{x},\mathbf{h})=2r(\mathbf{x})/v^2(\mathbf{x}), \tag{2.7}$$

followed by the extended common offset modeling operator.

The common offset migration operator is the adjoint of this integral operator: its output is the offset-dependent prestack image volume, a function of the same type as the extended common offset reflectivity:

$$\begin{aligned}&\bar{F}^*_{\rm co}[v]d(\mathbf{x},\mathbf{h})=I_{\rm co}(\mathbf{x},\mathbf{h}),\\ &I_{\rm co}(\mathbf{x},\mathbf{h})=\int d\mathbf{x}_m\int dt\frac{\partial^2 d}{\partial t^2}(\mathbf{x}_m+\mathbf{h},t;\mathbf{x}_m-\mathbf{h})\int d\tau\,G(\mathbf{x},t-\tau;\mathbf{x}_m+\mathbf{h})G(\mathbf{x},\tau;\mathbf{x}_m-\mathbf{h}).\end{aligned} \tag{2.8}$$

Therefore the adjoint of Born modeling (migration, *per se*) is common offset migration followed by the adjoint of the "spray" operator: this adjoint is the operator which sums or integrates in $\mathbf{h}$, that is, the *stack* operator.

Actually the operator defined in equation 2.8 is only one possible common offset migration operator. Many others follow through application of various weights, filters, and approximations. For example, leaving off the second time derivative in equation 2.8 amounts to filtering the data before application of $\bar{F}^*_{\rm co}[v]$. Most notably, replacement of the Green's functions in equation 2.8 by the leading terms in their high frequency asymptotic expansions results in the familiar Kirchhoff

common offset migration operator. All of these variations define adjoints to (approximations of) the modeling operator with respect to appropriate inner products on domain and range spaces. Most important for this investigation, all share a common kinematic description. Therefore we ignore all such variations for the time being, and refer to equation 2.8 as defining "the" common offset migration operator.

Note that both modeling and migration operators share the property that their output for a given $\mathbf{h}$ depends only on the input for the same value of $\mathbf{h}$ - that is, they are *block-diagonal* on common offset data bins. This binwise action is responsible for the production of kinematic artifacts when the velocity field refracts rays sufficiently strongly [33].

2.3. Shot-geophone modeling and migration. Shot-geophone modeling results from a different extension of reflectivity: replace $2r(\mathbf{x})/v^2(\mathbf{x})$ by $R(\mathbf{x},\mathbf{h})$ where $\mathbf{h}$ is the subsurface (half)offset mentioned in the introduction. While this extension has exactly the same degrees of freedom as the common offset extended reflectivity, the two are conceptually quite different: $\mathbf{h}$ here has *nothing to do* with the surface source-receiver half-offset $\frac{1}{2}(\mathbf{x}_r - \mathbf{x}_s)$!

The shot-geophone modeling operator $\bar{F}[v]$ is given by

$$\bar{F}[v]R(\mathbf{x}_r,t;\mathbf{x}_s) = u(\mathbf{x}_r,t;\mathbf{x}_s), \tag{2.9}$$

where the field u is defined by

$$u(\mathbf{x}_r,t;\mathbf{x}_s) = \frac{\partial^2}{\partial t^2}\int d\mathbf{x}\int d\mathbf{h}\, R(\mathbf{x},\mathbf{h})\int d\tau\, G(\mathbf{x}+\mathbf{h},t-\tau;\mathbf{x}_r)G(\mathbf{x}-\mathbf{h},\tau;\mathbf{x}_s). \tag{2.10}$$

Note that here $\mathbf{x}$ does play the role of subsurface midpoint, though having nothing to do with surface source-receiver midpoint.

The field $u(\mathbf{x},t;\mathbf{x}_s)$ is identical to $\delta G(\mathbf{x},t;\mathbf{x}_s)$ when

$$R(\mathbf{x},\mathbf{h}) = \frac{2r(\mathbf{x})}{v^2(\mathbf{x})}\delta(\mathbf{h}), \tag{2.11}$$

i.e. when the generalized reflectivity is concentrated at offset zero. Therefore Born modeling is shot-geophone modeling following the mapping

$$r(\mathbf{x}) \mapsto \frac{2r(\mathbf{x})}{v^2(\mathbf{x})}\delta(\mathbf{h}). \tag{2.12}$$

The shot-geophone migration operator is the adjoint of the shot-geophone modeling operator: it produces an image volume with the same degrees of freedom as the extended shot-geophone reflectivity,

$$\bar{F}^*[v]d(\mathbf{x},\mathbf{h}) = I_{\mathrm{s-g}}(\mathbf{x},\mathbf{h}),$$

$$I_{\mathrm{s-g}}(\mathbf{x},\mathbf{h}) = \int d\mathbf{x}_r\int d\mathbf{x}_s\int dt\,\frac{\partial^2 d}{\partial t^2}(\mathbf{x}_r,t;\mathbf{x}_s)\int d\tau\, G(\mathbf{x}+\mathbf{h},t-\tau;\mathbf{x}_r)G(\mathbf{x}-\mathbf{h},\tau;\mathbf{x}_s). \tag{2.13}$$

Note that in both equations 2.10 and 2.13, all input variables are integrated to produce the value at each output vector: the computation is not block diagonal in $\mathbf{h}$, in contrast to the common offset operators defined in equations 2.6 and 2.8.

Born migration is shot-geophone migration followed by the adjoint of the mapping defined in equation 2.12, which is

$$R(\mathbf{x},\mathbf{h}) \mapsto \frac{2R(\mathbf{x},0)}{v^2(\mathbf{x})}, \tag{2.14}$$

in other words, shot-geophone migration followed by extraction of the zero offset section.

For some purposes it turns out to be convenient to introduce *sunken source and receiver coordinates*

$$\bar{\mathbf{x}}_r = \mathbf{x} + \mathbf{h},\ \bar{\mathbf{x}}_s = \mathbf{x} - \mathbf{h}, \tag{2.15}$$

and the *source-receiver reflectivity* $\bar{R}$ by

$$\bar{R}(\bar{\mathbf{x}}_r, \bar{\mathbf{x}}_s) = R\left(\frac{\bar{\mathbf{x}}_r + \bar{\mathbf{x}}_s}{2}, \frac{\bar{\mathbf{x}}_r - \bar{\mathbf{x}}_s}{2}\right),\ \text{i.e. } \bar{R}(\mathbf{x}+\mathbf{h}, \mathbf{x}-\mathbf{h}) = R(\mathbf{x}, \mathbf{h}), \tag{2.16}$$

and similarly for the image volume $I_{\mathrm{s-g}}$. Change integration variables in equation 2.13 to get the sunken source-receiver variant of shot-geophone migration:

$$\bar{I}_{\mathrm{s-g}}(\bar{\mathbf{x}}_r, \bar{\mathbf{x}}_s) = \int d\mathbf{x}_r \int d\mathbf{x}_s \int dt\, \frac{\partial^2 d}{\partial t^2}(\mathbf{x}_r, t; \mathbf{x}_s) \int d\tau\, G(\bar{\mathbf{x}}_r, t-\tau; \mathbf{x}_r) G(\bar{\mathbf{x}}_s, \tau; \mathbf{x}_s). \tag{2.17}$$

Replacement of the Green's functions in this formula by their high-frequency asymptotic (ray-theoretic) approximations results in a Kirchhoff-like representation of shot-geophone migration.

2.4. Adjoint state formulation. Equation 2.17 can be reproduced by solving (forward in time) the wave equation for the source field, w_s,

$$\frac{1}{v^2(\mathbf{x})}\frac{\partial^2 w_s}{\partial t^2}(\mathbf{x}, t; \mathbf{x}_s) - \nabla^2_{\mathbf{x}} w_s(\mathbf{x}, t; \mathbf{x}_s) = \delta(t)\delta(\mathbf{x} - \mathbf{x}_s), \tag{2.18}$$

in parallel with solving (backward in time) the wave equation for the adjoint field, u^*,

$$\frac{1}{v^2(\mathbf{x})}\frac{\partial^2 u^*}{\partial t^2}(\mathbf{x}, t; \mathbf{x}_s) - \nabla^2_{\mathbf{x}} u^*(\mathbf{x}, t; \mathbf{x}_s) = \int d\mathbf{x}\, \frac{\partial^2 d}{\partial t^2}(\mathbf{x}_r, t; \mathbf{x}_s)\delta(\mathbf{x} - \mathbf{x}_r), \tag{2.19}$$

followed by the cross correlation at zero time lag,

$$\bar{I}_{\mathrm{s-g}}(\bar{\mathbf{x}}_r, \bar{\mathbf{x}}_s) = \int d\mathbf{x}_s \int d\tau\, u^*(\bar{\mathbf{x}}_r, \tau; \mathbf{x}_s) w_s(\bar{\mathbf{x}}_s, \tau; \mathbf{x}_s). \tag{2.20}$$

(An implementation of this formulation (i) avoids asymptotic approximations inherent in the downward-continuation formulation, and (ii) admits, in principle, highly irregular source and receiver spacing as these appear in global earth applications.)

3. Kinematics of shot-geophone migration. An event in the data is characterized by its moveout: locally, by a moveout equation $t = T(\mathbf{x}_r, \mathbf{x}_s)$, and infinitesimally by the source and receiver slownesses

$$\mathbf{p}_r = \nabla_{\mathbf{x}_r} T,\ \mathbf{p}_s = \nabla_{\mathbf{x}_s} T \tag{3.1}$$

Significant energy with this moveout implies that locally near $(\mathbf{x}_r, \mathbf{x}_s, t)$ the data contains a plane wave component with wavenumber $(\omega\mathbf{p}_r, \omega\mathbf{p}_s, \omega)$, ω being temporal frequency. These coordinates (position, wavenumber) give the (geometrical) phase space representation of the event.

Note that for incomplete coverage, an event in the data will typically not determine its moveout uniquely. For example, in conventional marine streamer geometry, with the streamers oriented along the x axis, the y component of $\mathbf{p}_r$ is not determined by the data. However, in present day (possibly zigzag) WATS acquisition geometry [19, 3], $\mathbf{p}_r$, and $\mathbf{p}_s$, are determined. In the discussion to follow, $\mathbf{p}_s$ and $\mathbf{p}_r$ are assumed to be *compatible* with a reflection event. Likewise, a reflector (in the source-receiver representation) at $(\bar{\mathbf{x}}_r, \bar{\mathbf{x}}_s)$ with wavenumber $(\mathbf{k}_r, \mathbf{k}_s)$ is characterized in (image volume) phase space by these coordinates.

3.1. Kinematics with general (3D) subsurface offset. The kinematical description of shot-geophone migration relates the phase space coordinates of events and reflectors. An event or reflection with phase space representation

$$(\mathbf{x}_r, \mathbf{x}_s, T(\mathbf{x}_r, \mathbf{x}_s), \omega\mathbf{p}_r, \omega\mathbf{p}_s, \omega) \tag{3.2}$$

is the result of a reflector with (source-receiver) phase space representation $(\bar{\mathbf{x}}_r, \bar{\mathbf{x}}_s, \mathbf{k}_r, \mathbf{k}_s)$ exactly when

- there is a ray $(\mathbf{X}_s, \mathbf{P}_s)$ leaving the source point $\mathbf{X}_s(0) = \mathbf{x}_s$ at time $t = 0$ with ray parameter $\mathbf{P}_s(0) = \mathbf{p}_s$, and arriving at $\mathbf{X}_s(t_s) = \bar{\mathbf{x}}_s$ at $t = t_s$ with ray parameter $\mathbf{P}_s(t_s) = -\mathbf{k}_s/\omega$;
- there is a ray $(\mathbf{X}_r, \mathbf{P}_r)$ leaving $\mathbf{X}_r(t_s) = \bar{\mathbf{x}}_r$ at $t = t_s$ with ray parameter $\mathbf{P}_r(t_s) = \mathbf{k}_r/\omega$ and arriving at the receiver point $\mathbf{X}_r(t_r + t_s) = \mathbf{x}_s$ at time $t = T(\mathbf{x}_r, \mathbf{x}_s) = t_r + t_s$ with ray parameter $\mathbf{P}_r(t_r + t_s) = \mathbf{p}_r$.

Figure 1 illustrates this kinematic relation. The Appendix provides a derivation.

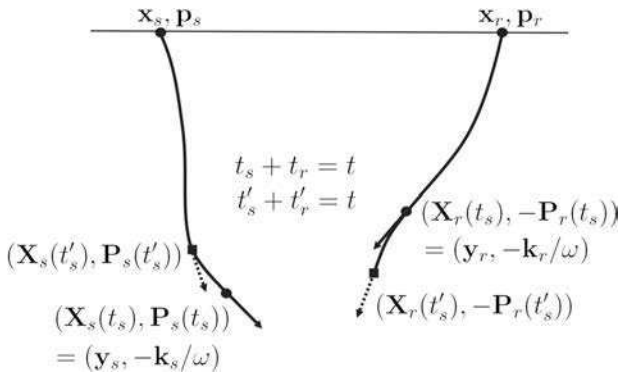

FIGURE 1. *Ray theoretic relation between data event and double reflector.*

Note that since $\mathbf{P}_r, \mathbf{P}_s$ are ray slowness vectors, there is necessarily a length relation between $\mathbf{k}_r, \mathbf{k}_s$: namely,

$$\begin{aligned} \frac{1}{v(\bar{\mathbf{x}}_r)} &= \|\mathbf{P}_r(t_r)\| = \frac{\|\mathbf{k}_r\|}{|\omega|}, \\ \frac{1}{v(\bar{\mathbf{x}}_s)} &= \|\mathbf{P}_s(t_s)\| = \frac{\|\mathbf{k}_s\|}{|\omega|}, \end{aligned} \tag{3.3}$$

whence

$$\frac{\|\mathbf{k}_r\|}{\|\mathbf{k}_s\|} = \frac{v(\bar{\mathbf{x}}_s)}{v(\bar{\mathbf{x}}_r)} \tag{3.4}$$

The kinematics of shot-geophone migration are somewhat strange, so it is reassuring to see that for physical reflectors (i.e. $R(\mathbf{x}, \mathbf{h}) = r(\mathbf{x})\delta(\mathbf{h})$) the relation just explained becomes the familiar one of reflection from a reflecting element according to Snell's law. A quick calculation shows that such a physical $\bar{R}$ has a significant local plane wave component near $(\bar{\mathbf{x}}_r, \bar{\mathbf{x}}_s)$ with wavenumber $(\mathbf{k}_r, \mathbf{k}_s)$ only if $\bar{\mathbf{x}}_r = \bar{\mathbf{x}}_s = \mathbf{x}$ and r has a significant local plane wave component near $\mathbf{x}$ with wavenumber $\mathbf{k}_x = \mathbf{k}_r + \mathbf{k}_s$. From equation 3.4, $\mathbf{k}_r$ and $\mathbf{k}_s$ have the same length, therefore their sum $\mathbf{k}_x$ is also their bisector, which establishes Snell's law. Thus a single (physical) reflector at $\mathbf{x}$ with wavenumber $\mathbf{k}_x$ gives rise to a reflected event at frequency ω exactly when the rays $(\mathbf{X}_s, \mathbf{P}_s)$ and $(\mathbf{X}_r, \mathbf{P}_r)$ meet at $\mathbf{x}$ at time t_s, and the reflector dip $\mathbf{k}_x = \omega(\mathbf{P}_r(t_s) - \mathbf{P}_s(t_s))$, which is the usual kinematics of single scattering. See Figure 2.

It is now possible to answer the question: in the shot-geophone model, to what extent does a data event determine the corresponding reflector? The rules derived above show that the reflection

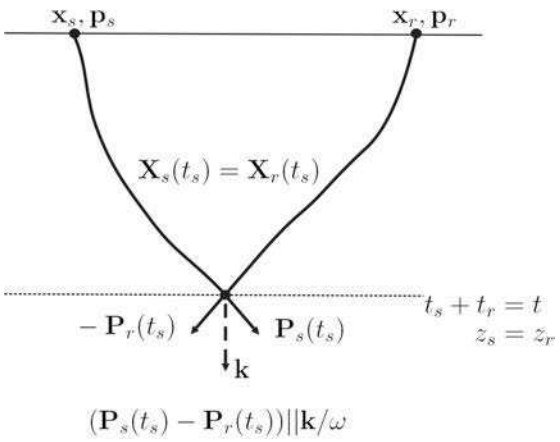

FIGURE 2. *Ray theoretic relation between data event and physical (single) reflector.*

point $(\bar{\mathbf{x}}_s, \bar{\mathbf{x}}_r)$ must lie on the Cartesian product of two rays, $(\mathbf{X}_s, \mathbf{P}_s)$ and $(\mathbf{X}_r, \mathbf{P}_r)$, consistent with the event, and the total time is also determined. If the coverage is complete, so that the event uniquely determines the source and receiver rays, then the source-receiver representation of the source-receiver reflector must lie along this uniquely determined ray pair. This fact contrasts dramatically with the imaging ambiguities prevalent in all forms of prestack depth migration based on data binning [20, 21, 37, 22, 7, 34, 33]. Even when coverage is complete, in these other forms of prestack migration strong refraction leads to multiple ray pairs connecting data events and reflectors, whence ambiguous imaging of a single event in more than one location within the prestack image volume.

Nonetheless reflector location is still not uniquely determined by shot-geophone migration as defined above, for two reasons:

- Only the total traveltime is specified by the event! Thus if $\bar{\mathbf{x}}_s = \mathbf{X}_s(t_s), \bar{\mathbf{x}}_r = \mathbf{X}_r(t_s)$ are related as described above to the event determining the ray pair, so is $\bar{\mathbf{x}}'_s = \mathbf{X}_s(t'_s), \bar{\mathbf{x}}'_r = \mathbf{X}_r(t'_s)$ with $t_s + t_r = t'_s + t'_r = t_{sr}$. See Figure 1.
- Incomplete acquisition, for example limited to a narrow azimuth range, may prevent the event from determining its full 3D moveout, as mentioned above. Therefore a family of ray pairs, rather than a unique ray pair, may correspond to the event.

3.2. Kinematics with horizontal subsurface offset. One way to view the remaining imaging ambiguity in shot-geophone migration as defined so far is to recognize that the image point coordinates $(\bar{\mathbf{x}}_r, \bar{\mathbf{x}}_s)$ (or $(\mathbf{x}, \mathbf{h})$) are six-dimensional (in 3D), whereas the data depend on only five coordinates $(\mathbf{x}_r, t, \mathbf{x}_s)$ (at most). Formally, restricting one of the coordinates of the image point to be zero would at least make the variable counts equal, so that unambiguous imaging would at least be conceivable. Since physical reflectivities are concentrated at zero (vector) offset, it is natural to restrict one of the offset coordinates to be zero. The conventional choice, beginning with Claerbout's definition of survey-sinking migration [9], is the depth coordinate.

We assume that the shot-geophone reflectivity $R(\mathbf{x}, \mathbf{h})$ takes the form

$$R(\mathbf{x}, \mathbf{h}) = R_z(\mathbf{x}, h_x, h_y)\delta(h_z), \tag{3.5}$$

leading to the restricted modeling operator:

$$\bar{F}_z[v]R_z(\mathbf{x}_r, t; \mathbf{x}_s) = \frac{\partial^2}{\partial t^2} \int d\mathbf{x} \int dh_x \int dh_y$$

$$R_z(\mathbf{x}, h_x, h_y) \int d\tau\, G(\mathbf{x} + (h_x, h_y, 0), t - \tau; \mathbf{x}_r) G(\mathbf{x} - (h_x, h_y, 0), \tau; \mathbf{x}_s) \tag{3.6}$$

(cf. equations 2.9-2.10). The kinematics of this restricted operator follows directly from that of the unrestricted operator, developed in the preceding section.

Denote $\bar{\mathbf{x}}_s = (\bar{x}_s, \bar{y}_s, \bar{z}_s), \mathbf{k}_s = (k_{s,x}, k_{s,y}, k_{s,z})$ etc. For horizontal offset, the restricted form of the reflectivity in midpoint-offset coordinates (equation 3.5) implies a similarly restricted form for its description in sunken source-receiver coordinates:

$$\bar{R}(\bar{\mathbf{x}}_r, \bar{\mathbf{x}}_s) = \bar{R}_z \left(\bar{x}_r, \bar{x}_s, \bar{y}_r, \bar{y}_s, \frac{\bar{z}_r + \bar{z}_s}{2} \right) \delta(\bar{z}_r - \bar{z}_s). \tag{3.7}$$

Fourier transformation shows that $\bar{R}$ has a significant plane wave component with wavenumber $(\mathbf{k}_r, \mathbf{k}_s)$ precisely when $\bar{R}_z$ has a significant plane wave component with wavenumber $k_{r,x}, k_{r,y}, k_{s,x}, k_{s,y}, (k_{r,z}+k_{s,z})$. Thus a ray pair $(\mathbf{X}_r, \mathbf{P}_r), (\mathbf{X}_s, \mathbf{P}_s)$ compatible with a data event with phase space coordinates $(\mathbf{x}_r, \mathbf{x}_s, T(\mathbf{x}_r, \mathbf{x}_s), \omega \mathbf{p}_r, \omega \mathbf{p}_s, \omega)$ images at a point $X_{r,z}(t_s) = X_{s,z}(t_s) = z$, $P_{r,z}(t_s) - P_{s,z}(t_s) = k_z/\omega$, $X_{s,x}(t_s) = x_s$, $P_{s,x}(t_s) = k_{s,x}/\omega$, etc. at image phase space point

$$(\bar{x}_r, \bar{x}_s, \bar{y}_r, \bar{y}_s, z, k_{r,x}, k_{s,x}, k_{r,y}, k_{s,y}, k_z). \tag{3.8}$$

The adjoint of the modeling operator defined in equation 3.6 is the horizontal offset shot-geophone migration operator:

$$\bar{F}_z^*[v] d(\mathbf{x}, h_x, h_y) = I_{\mathrm{s-g,z}}(\mathbf{x}, h_x, h_y), \tag{3.9}$$

where

$$I_{\mathrm{s-g,z}}(\mathbf{x}, h_x, h_y) = \int d\mathbf{x}_r \int d\mathbf{x}_s \int dt$$

$$\frac{\partial^2}{\partial t^2} d(\mathbf{x}_r, t; \mathbf{x}_s) \int d\tau \, G(\mathbf{x} + (h_x, h_y, 0), t - \tau; \mathbf{x}_r) G(\mathbf{x} - (h_x, h_y, 0), \tau; \mathbf{x}_s). \tag{3.10}$$

As mentioned before, operators and their adjoints enjoy the same kinematic relations, so we have already described the kinematics of this migration operator.

3.3. Semblance property of horizontal offset image gathers and the DSR condition. As explained by Stolk and De Hoop [30], Claerbout's survey sinking migration is kinematically equivalent to shot-geophone migration as defined here, under two assumptions:

- subsurface offsets are restricted to horizontal ($h_z = 0$);
- rays (either source or receiver) carrying significant energy are nowhere horizontal, i.e. $P_{s,z} > 0, P_{r,z} < 0$ throughout the propagation;
- events in the data determine full (four-dimensional) slowness $\mathbf{P}_r, \mathbf{P}_s$.

We call the second condition the "Double Square Root", or "DSR", condition, for reasons explained by Stolk and De Hoop [30]. This reference also offers a proof of the

Claim: Under these restrictions, the imaging operator $\bar{F}_z^*$ can image a ray pair at precisely one location in image volume phase space. When the velocity is correct, the image energy is therefore concentrated at zero offset in the image volume $I_{\mathrm{s-g,z}}$.

The demonstration presented by Stolk and De Hoop [30] uses oscillatory integral representations of the operator $\bar{F}_z$ and its adjoint. However, the conclusion also follows directly from the kinematic analysis above and the DSR condition.

Indeed, note that the DSR condition implies that depth is increasing along the source ray, and decreasing along the receiver ray - otherwise put, depth is increasing along both rays, if you traverse the receiver ray *backwards*. Therefore depth can be used to parametrize the rays. With depth as the parameter, time is increasing from zero along the source ray, and decreasing from t_{sr} along the receiver ray (traversed backwards). Thus the two times can be equal (to t_s) at exactly one point.

Since the scattering time t_s is uniquely determined, so are all the other phase space coordinates of the rays. If the ray pair is the incident-reflected ray pair of a reflector, then the reflector must be the *only* point at which the rays cross, since there is only one time t_s at which $X_{s,z}(t_s) = X_{r,z}(t_s)$. See Figure 3. Therefore in the infinite frequency limit the energy of this incident-reflected ray pair is imaged at zero offset, consistent with Claerbout's imaging condition.

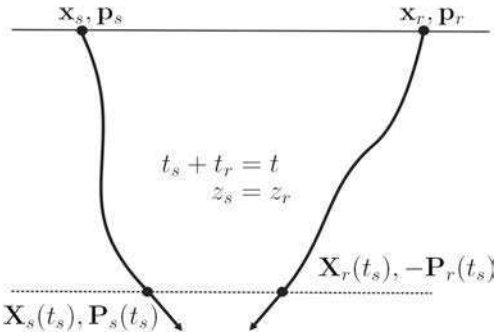

FIGURE 3. *Ray geometry for double reflector with horizontal offset only.*

If furthermore coverage is complete, whence the data event uniquely determines the full slowness vectors, hence the rays, then it follows that a data event is imaged at precisely one location, namely the reflector which caused it, and in particular focusses at zero offset. This is the offset version of the result established by Stolk and De Hoop [30], for which we have now given a different (and more elementary) proof.

3.4. Semblance property of angle image gathers via Radon transform in offset and depth. According to Sava and Fomel [25], angle image gathers A_z may be defined via a Radon transform in offset and depth of the offset image gathers constructed above, i.e. the migrated data volume $I_{\mathrm{s-g,z}}(\mathbf{x}, h_x, h_y)$ (defined in equation 3.10) for fixed x, y:

$$A_z(x, y, \zeta, p_x, p_y) = \int dh_x \int dh_y \, I_{\mathrm{s-g,z}}(x, y, \zeta + p_x h_x + p_y h_y, h_x, h_y), \tag{3.11}$$

in which ζ denotes the z-intercept parameter, and p_x and p_y are the x and y components of offset ray parameter. The ray parameter components may then be converted to angle [25]. As is obvious from this formula, if the energy in $I_{\mathrm{s-g,z}}(\mathbf{x}, h_x, h_y)$ is focussed, i.e. localized, on $h_x = 0, h_y = 0$, then the Radon transform A_z will be (essentially) independent of p_x, p_y. That is, when displayed for fixed x, y with ζ axis plotted vertically and p_x and p_y horizontally, the events in A_z will appear *flat*. The converse is also true. This is the semblance principle for angle gathers.

4. Semblance property of angle gathers via Radon transform in offset and time. The angle gathers defined by De Bruin et al. [10] are based on migrated data $D(\mathbf{x}, h_x, h_y, T)$, i.e. depending on a time variable T in addition to the variables $(\mathbf{x}, h_x, h_y)$. Such migrated data are for example given by the following modification of equation 3.10

$$\begin{aligned} D(\mathbf{x}, h_x, h_y, T) = &\int d\mathbf{x}_s \int d\mathbf{x}_r \int dt \\ &\frac{\partial^2}{\partial t^2} d(\mathbf{x}_r, t; \mathbf{x}_s) \int d\tau \, G(\mathbf{x} + (h_x, h_y, 0), t - T - \tau; \mathbf{x}_r) G(\mathbf{x} - (h_x, h_y, 0), \tau; \mathbf{x}_s) \\ &= \int d\mathbf{x}_s \int d\tau \, u^*(\mathbf{x} + (h_x, h_y, 0), T + \tau; \mathbf{x}_s) w_s(\mathbf{x} - (h_x, h_y, 0), \tau; \mathbf{x}_s) \end{aligned} \tag{4.1}$$

(which represents a successive evaluation of laterally shifted time correlations accumulated over all shots; cf. equations 2.18 and 2.19). As we have done with other fields, we denote by $\bar{D}$ the field D referred to sunken source and receiver coordinates.

Again this migration formula can be obtained as the adjoint of a modified forward map, mapping an extended reflectivity to data, similarly as above. In this case the extended reflectivity depends on the variables $(\mathbf{x}, h_x, h_y, T)$, with physical reflectivity given by $r(\mathbf{x})\delta(h_x)\delta(h_y)\delta(T)$. This physical reflectivity is obtained by a time injection operator

$$(J_t \bar{R}_z)(\bar{x}_r, \bar{x}_s, \bar{y}_r, \bar{y}_s, \bar{z}, t) = \bar{R}_z(\bar{x}_r, \bar{x}_s, \bar{y}_r, \bar{y}_s, \bar{z})\delta(t). \tag{4.2}$$

To obtain a migrated image volume, the extraction of zero offset data in equation 2.14 is preceded by extracting the $T = 0$ data from D. It is indeed clear that setting T to zero in equation 4.1 yields the shot-geophone migration output defined in equation 3.10.

4.1. Wave-equation angle transform. Angle gathers obtained via Radon transform in offset and time of $D(\mathbf{x}, h_x, h_y, T)$ were introduced by [10], and discussed further in [22]. We denote these gathers by

$$B_z(\mathbf{x}, p_x, p_y) = \int dh_x \int dh_y \, D(\mathbf{x}, h_x, h_y, p_x h_x + p_y h_y)\, \chi(h), \tag{4.3}$$

where $\chi(h)$ is an appropriately chosen tapered mute restricting the range of h values [30]. The ray parameter components may be converted to angle [12]. The purpose of this section is to establish the semblance property of the angle gathers B_z.

Note that the Radon transform in equation 4.3 is evaluated at zero (time) intercept. The dependence on z is carried by the coordinate plane in which the Radon transform is performed, rather than by the $(z-)$ intercept as was the case with the angle gathers A_z defined previously. Also note that B_z requires the field D, whereas A_z may be constructed with the image output.

We first need to establish at which points $(\mathbf{x}, h_x, h_y, T)$ significant energy of $D(\mathbf{x}, h_x, h_y, T)$ is located. The argument for $\bar{D}$ is slightly different from the argument for $\bar{I}_z$, since $\bar{D}$ depends also on the time. For $\bar{I}_z$ there was a kinematic relation $(\mathbf{x}_s, \mathbf{x}_r, t_{sr}, \omega\mathbf{p}_s, \omega\mathbf{p}_r, \omega)$ to a point in phase space $(x_s, x_r, y_s, y_r, z, k_{s,x}, k_{r,x}, k_{s,y}, k_{r,y}, k_z)$ where the energy in $\bar{I}_z$ is located. The restriction of $\bar{D}$ to time T is the same as the restriction to time 0, but using time-shifted data $d(..., t+T)$. Therefore we can follow almost the same argument as for the kinematic relation of $\bar{I}_z$. We find that for an event at $(\mathbf{x}_s, \mathbf{x}_r, t_{sr}, \omega\mathbf{p}_s, \omega\mathbf{p}_r, \omega)$ to contribute at $\bar{D}$, restricted to time T, we must have that (x_s, y_s, z) is on the ray $\mathbf{X}_s$, say at time t'_s, i.e. $(x_s, y_s, z) = \mathbf{X}_s(t'_s)$. Then (x_r, y_r, z) must be on the ray $\mathbf{X}_r$ say at time t''_s, i.e. $(x_r, y_r, z) = \mathbf{X}_r(t''_s)$. The situation is displayed in Figure 4, using midpoint-offset coordinates. Furthermore, the sum of the traveltimes from $\mathbf{x}_s$ to (x_s, y_s, z) and from $\mathbf{x}_r$ to (x_r, y_r, z) must be equal to $t_{sr} - T$. It follows that $t''_s - t'_s = T$.

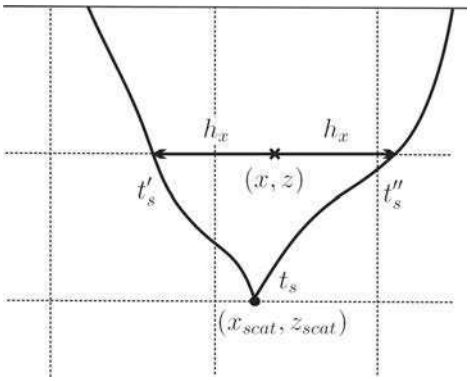

FIGURE 4. *Ray geometry for offset-time angle gather construction.*

Now consider an event from a physical reflection at $\mathbf{X}_s(t_s) = \mathbf{X}_r(t_s) = (x_{\text{scat}}, y_{\text{scat}}, z_{\text{scat}})$. We use the previous reasoning to find where the energy in D is located (in midpoint-offset coordinates).

We will denote by $(v_{s,x}(t), v_{s,y}(t), v_{s,z}(t))$ the ray velocity for the source ray $\frac{d\mathbf{X}_s}{dt}$. The horizontal "sunken source" coordinates $(x - h_x, y - h_y)$ then satisfy

$$x_{\text{scat}} - (x - h_x) = \int_{t'_s}^{t_s} dt\, v_{s,x}(t), \quad y_{\text{scat}} - (y - h_y) = \int_{t'_s}^{t_s} dt\, v_{s,y}(t), \tag{4.4}$$

For the "sunken receiver" coordinates we find

$$(x + h_x) - x_{\text{scat}} = \int_{t_s}^{t''_s} dt\, v_{r,x}(t), \quad (y + h_y) - y_{\text{scat}} = \int_{t_s}^{t''_s} dt\, v_{r,y}(t). \tag{4.5}$$

Adding up the x components of these equations, and separately the y components of these equations gives that

$$2h_x = \int_{t'_s}^{t''_s} v_x(t)dt, \quad 2h_y = \int_{t'_s}^{t''_s} v_y(t)dt, \tag{4.6}$$

where now the velocity $(v_x(t), v_y(t))$ is from the source ray for $t < t_s$, and from the receiver ray for $t > t_s$. Let us denote by $v_{\|,\max}$ the maximal horizontal velocity along the rays between $(x_{\text{scat}}, y_{\text{scat}}, z_{\text{scat}})$ and the points (x_s, y_s, z) and (x_r, y_r, z), then we have

$$2\|(h_x, h_y)\| \leq |t''_s - t'_s| v_{\|,\max} = |T| v_{\|,\max}. \tag{4.7}$$

For the 2D case we display the situation in Figure 5. The energy in $\bar{D}$ is located in the shaded region of the (h_x, T) plane indicated in the Figure. In 3D this region becomes a cone.

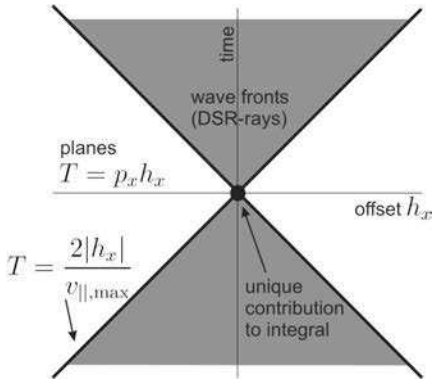

FIGURE 5. *Cone in phase space for energy admitted to angle gather construction.*

The angle transform in equation 4.3 is an integral of D over a plane in the (h_x, h_y, T) volume given by

$$T = p_x h_x + p_y h_y. \tag{4.8}$$

Suppose now that

$$\sqrt{p_x^2 + p_y^2} < \frac{2}{v_{\|,\max}}, \tag{4.9}$$

Then we have

$$|T| = |p_x h_x + p_y h_y| < \frac{2}{v_{\|,\max}} \sqrt{h_x^2 + h_y^2}. \tag{4.10}$$

In the 2D Figure 5 this means that the lines of integration are not in the shaded region of the (h_x, T) plane. In 3D, the planes of integration are not in the corresponding cone. The only points where the planes of integration intersect the set of (h_x, h_y, T) where energy of D is located, are points with $T = 0, h_x = h_y = 0$. It follows that the energy in the angle transform of equation 4.3 is located only at the true scattering point independent of (p_x, p_y). We conclude that the semblance property also holds for the angle transform via Radon transform in the offset time domain, provided that 4.9 holds.

The bound $v_{\|,\max}$ need not be a global bound on the horizontal component of the ray velocity. The integral in equation 4.3 is over some finite range of offsets, hence on some finite range of times, so that the distance between say the midpoint $\mathbf{x}$ in equation 4.3, and the physical scattering point is bounded. Therefore $v_{\|,\max}$ should be a bound on the horizontal component of the ray velocity on some sufficiently large region around $\mathbf{x}$.

4.2. Pseudodepth and turning rays. The analysis developed above can be generalized to accommodate a large class of turning rays. To this end, we introduce curvilinear coordinates and the notion of pseudodepth (see [26]) which will lead to the curvilinear DSR condition.

In our notation, here, we distinguish between horizontal coordinates $x_\sigma = (x, y)_\sigma$ ($\sigma = 1, 2$) and the vertical coordinate z. Similarly the curvilinear coordinates are denoted by $(\tilde{x}, \tilde{y}, \tilde{z})$ and we write $\tilde{x}_\sigma = (\tilde{x}, \tilde{y})_\sigma$ for the "horizontal" coordinates; $\tilde{z}$ will represent pseudodepth.

We will need the metric, $\tilde{g}$, associated with the new coordinates. With the original (flat) coordinates we associate the metric $g_{ij} = \delta_{jk}$ (we will use upper and lower indices as in Riemannian geometry). Then

$$\tilde{g}_{il} = \frac{\partial(x, y, z)^j}{\partial(\tilde{x}, \tilde{y}, \tilde{z})^i} \delta_{jk} \frac{\partial(x, y, z)^k}{\partial(\tilde{x}, \tilde{y}, \tilde{z})^l}$$

with associated volume element $|\det \tilde{g}|^{1/2} d\tilde{x} d\tilde{y} d\tilde{z} = |\frac{\partial(x,y,z)}{\partial(\tilde{x},\tilde{y},\tilde{z})}| \, d\tilde{x} d\tilde{y} d\tilde{z}$. We employ the summation convention: summation over repeated indices is implicit (in other words, this equation is a shorthand for $\tilde{g}_{il} = \sum_{j,k=1}^{3} \frac{\partial(x,y,z)^j}{\partial(\tilde{x},\tilde{y},\tilde{z})^i} \delta_{jk} \frac{\partial(x,y,z)^k}{\partial(\tilde{x},\tilde{y},\tilde{z})^l}$). The inverse metric equals

$$\tilde{g}^{il} = \frac{\partial(\tilde{x}, \tilde{y}, \tilde{z})^i}{\partial(x, y, z)^j} \delta^{jk} \frac{\partial(\tilde{x}, \tilde{y}, \tilde{z})^l}{\partial(x, y, z)^k}.$$

The coordinate $\tilde{z}$ defines a local pseudodepth if $\frac{\partial(x,y,z)}{\partial\tilde{x}} \perp \frac{\partial(x,y,z)}{\partial\tilde{z}}$ and $\frac{\partial(x,y,z)}{\partial\tilde{y}} \perp \frac{\partial(x,y,z)}{\partial\tilde{z}}$. Thus, the local pseudodepth, $\tilde{z}$, will play a special role, different from $(\tilde{x}, \tilde{y})$. We assume that a pseudodepth can be defined at least in target regions, where the metric $\tilde{g}_{ij}$ must be of the form

$$\tilde{g}_{ij} = \begin{pmatrix} \tilde{g}_{11} & \tilde{g}_{12} & 0 \\ \tilde{g}_{21} & \tilde{g}_{22} & 0 \\ 0 & 0 & \tilde{g}_{33} \end{pmatrix}_{ij}; \tag{4.11}$$

the inverse metric $\tilde{g}^{ij}$ is of the same form. Also, $\tilde{g}_{\sigma\sigma'}$ denotes the elements of the 2×2 matrix

$$\tilde{g}_{\sigma\sigma'} = \begin{pmatrix} \tilde{g}_{11} & \tilde{g}_{12} \\ \tilde{g}_{21} & \tilde{g}_{22} \end{pmatrix}_{\sigma\sigma'}$$

that is, the horizontal part of the metric. For our analysis we only need local coordinates and a Riemannian metric of the form (4.11).

The transformation of the acoustic wave equation is most naturally done using a variational formulation. This yields an action functional

$$S = \tfrac{1}{2} \int_a^b \iint \left(\kappa \left| \frac{\partial u}{\partial t} \right|^2 - \rho^{-1} \|\nabla u\|^2 + uf \right) dx \, dy \, dz \, dt,$$

where ρ is the volume density of mass, and κ is the compressibility whence $c^{-2} = \rho\kappa$. The wave equation follows from the Euler-Lagrange equations derived from this action. The variation of this action under v (the derivative if $u \to u + v$) can be written as

$$\begin{aligned}\delta_v S &= \int_a^b \iiint \left(\kappa \frac{\partial v}{\partial t} \frac{\partial u}{\partial t} - \rho^{-1} \nabla v \cdot \nabla u + v f \right) dx\, dy\, dz\, dt \\ &= \int_a^b \iiint v \left(-\kappa \frac{\partial^2 u}{\partial t^2} + \nabla \cdot (\rho^{-1} \nabla u) + f \right) dx\, dy\, dz\, dt,\end{aligned}$$

where the second step was obtained by integration by parts, using that $v = 0$ for $t = a$ and $t = b$. Since this must be true for all v, the wave equation follows.

We define the transformed wave field as $\tilde{u}(\tilde{x}, \tilde{y}, \tilde{z}) = u(x(\tilde{x}, \tilde{y}, \tilde{z}), y(\tilde{x}, \tilde{y}, \tilde{z}), z(\tilde{x}, \tilde{y}, \tilde{z}))$. To obtain the wave equation in the new coordinates (see also [16]), we transform the action. In the new coordinates it becomes

$$\begin{aligned}S = \tfrac{1}{2} \int_a^b \iiint \Bigg(\kappa \left| \frac{\partial \tilde{u}}{\partial t} \right|^2 - \rho^{-1} \left(\frac{\partial(\tilde{x}, \tilde{y}, \tilde{z})}{\partial(x, y, z)} \frac{\partial \tilde{u}}{\partial(\tilde{x}, \tilde{y}, \tilde{z})} \right) \cdot \left(\frac{\partial(\tilde{x}, \tilde{y}, \tilde{z})}{\partial(x, y, z)} \frac{\partial \tilde{u}}{\partial(\tilde{x}, \tilde{y}, \tilde{z})} \right) \\ + \tilde{u} f \Bigg) \left| \frac{\partial(x, y, z)}{\partial(\tilde{x}, \tilde{y}, \tilde{z})} \right| d\tilde{x}\, d\tilde{y} d\tilde{z}\, dt.\end{aligned}$$

By a similar argument as above, it follows that the wave equation has new coefficients (which are now anisotropic), $\kappa \left| \frac{\partial(x,y,z)}{\partial(\tilde{x},\tilde{y},\tilde{z})} \right|$ and $\rho^{-1} \left| \frac{\partial(x,y,z)}{\partial(\tilde{x},\tilde{y},\tilde{z})} \right| \tilde{g}^{ij}$, and reads

$$\kappa \left| \frac{\partial(x, y, z)}{\partial(\tilde{x}, \tilde{y}, \tilde{z})} \right| \frac{\partial^2 \tilde{u}}{\partial t^2} - \frac{\partial}{\partial(\tilde{x}, \tilde{y}, \tilde{z})^i} \left(\rho^{-1} \left| \frac{\partial(x, y, z)}{\partial(\tilde{x}, \tilde{y}, \tilde{z})} \right| \tilde{g}^{ij} \frac{\partial \tilde{u}}{\partial(\tilde{x}, \tilde{y}, \tilde{z})^j} \right) = f \left| \frac{\partial(x, y, z)}{\partial(\tilde{x}, \tilde{y}, \tilde{z})} \right| \tag{4.12}$$

or

$$\kappa \left| \frac{\partial(x, y, z)}{\partial(\tilde{x}, \tilde{y}, \tilde{z})} \right| \frac{\partial^2 \tilde{u}}{\partial t^2} - \frac{\partial}{\partial \tilde{z}} \left(\alpha \frac{\partial \tilde{u}}{\partial \tilde{z}} \right) - \frac{\partial}{\partial \tilde{x}^\sigma} \left(\rho^{-1} \left| \frac{\partial(x, y, z)}{\partial(\tilde{x}, \tilde{y}, \tilde{z})} \right| \tilde{g}^{\sigma\sigma'} \frac{\partial \tilde{u}}{\partial \tilde{x}^{\sigma'}} \right) = f \left| \frac{\partial(x, y, z)}{\partial(\tilde{x}, \tilde{y}, \tilde{z})} \right|, \tag{4.13}$$

with $\alpha = \rho^{-1} \tilde{g}^{33} \left| \frac{\partial(x,y,z)}{\partial(\tilde{x},\tilde{y},\tilde{z})} \right|$. In the case of flat coordinates the Green's function (cf. equation 2.1) satisfies equation 4.13 subject to the substitution $f = \rho\, \delta(\mathbf{x} - \mathbf{x}_s)\delta(t)$.

Asymptotic ray theory corresponding with the solutions of (4.12) is governed by the Hamiltonian, $\mathcal{H}$, obtained from the symbol of the wave operator on the left-hand side, which in curvilinear coordinates is given by

$$\begin{aligned}&\mathcal{H}(\tilde{x}, \tilde{y}, \tilde{z}, \tilde{p}_x, \tilde{p}_y, \tilde{p}_z) \\ &\qquad = \tfrac{1}{2} (\tilde{p}_x, \tilde{p}_y, \tilde{p}_z)_i \tilde{g}^{ij} c^2(x(\tilde{x}, \tilde{y}, \tilde{z}), y(\tilde{x}, \tilde{y}, \tilde{z}), z(\tilde{x}, \tilde{y}, \tilde{z}))(\tilde{p}_x, \tilde{p}_y, \tilde{p}_z)_j, \quad c^2 = (\rho\, \kappa)^{-1};\end{aligned} \tag{4.14}$$

here $(\tilde{p}_x, \tilde{p}_y, \tilde{p}_z)$ are the components of a slowness vector in curvilinear coordinates. Singularities propagate along rays, with tangent, or velocity, vectors given by

$$(\tilde{v}_x(t), \tilde{v}_y(t), \tilde{v}_z(t)) = \frac{\mathrm{d}\tilde{\mathbf{X}}}{\mathrm{d}t} = -\frac{\partial \mathcal{H}}{\partial(\tilde{p}_x, \tilde{p}_y, \tilde{p}_z)}. \tag{4.15}$$

Where the Riemannian metric attains the form (4.11), the $\tilde{x}$-velocity satisfies

$$\tilde{v}^\sigma(t) = c^2 \tilde{g}^{\sigma\sigma'} \tilde{\mathrm{P}}_{\sigma'}.$$

Moreover,

$$\frac{\mathrm{d}\tilde{\mathbf{P}}}{\mathrm{d}t} = \frac{\partial \mathcal{H}}{\partial(\tilde{x}, \tilde{y}, \tilde{z})}, \tag{4.16}$$

while the length of the slowness vector is such that $\mathcal{H}(\tilde{x},\tilde{y},\tilde{z},\tilde{p}_x,\tilde{p}_y,\tilde{p}_z)=\frac{1}{2}$.

Equation 4.3 is replaced by

$$B_z(\tilde{x},\tilde{y},\tilde{z},\tilde{p}_x,\tilde{p}_y)=\int dS(\tilde{h}_x,\tilde{h}_y)\,\tilde{D}(\tilde{x},\tilde{y},\tilde{z},\tilde{h}_x,\tilde{h}_y,\tilde{p}_\sigma\tilde{h}^\sigma)\,\chi(\tilde{h}_x,\tilde{h}_y), \tag{4.17}$$

where

$$dS(\tilde{h}_x,\tilde{h}_y)=|j(\tilde{h}_x,\tilde{h}_y)^T j(\tilde{h}_x,\tilde{h}_y)|^{1/2}\,d\tilde{h}_x d\tilde{h}_y,$$

in which

$$j(\tilde{h}_x,\tilde{h}_y)=\frac{\partial(\mathbf{x}_s,\mathbf{x}_r)}{\partial(\tilde{h}_x,\tilde{h}_y)},\quad \mathbf{x}_s=\mathbf{x}_s\underbrace{(\tilde{x}-\tilde{h}_x,\tilde{y}-\tilde{h}_y,\tilde{z})}_{=\tilde{\mathbf{x}}_s},\ \mathbf{x}_r=\mathbf{x}_r\underbrace{(\tilde{x}+\tilde{h}_x,\tilde{y}+\tilde{h}_y,\tilde{z})}_{=\tilde{\mathbf{x}}_r}$$

using that $\tilde{z}$ is a pseudodepth. We now assume that the source and receiver rays become nowhere horizontal in the curvilinear coordinate system. We refer to this assumption as the curvilinear DSR condition. We can then adapt the analysis exposed in equations 4.4-4.10.

While ignoring the $\tilde{z}$-component of velocity, it is immediate that

$$\tilde{v}^\sigma c^{-2}\tilde{g}_{\sigma\sigma'}\tilde{v}^{\sigma'}\le 1. \tag{4.18}$$

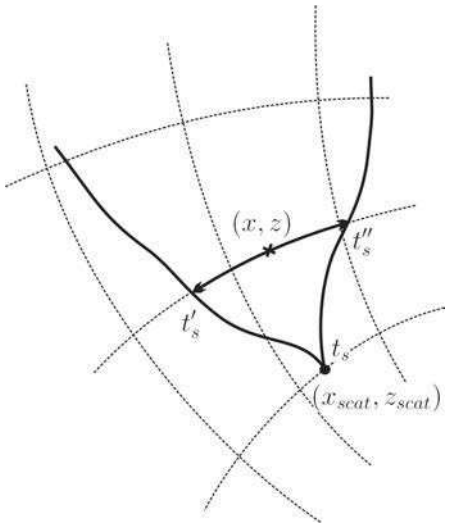

FIGURE 6. *Ray geometry for offset-time angle gather construction with respect to curvilinear coordinates.*

The relevant geometry is displayed in Figure 6. We now consider an event from a reflection at a point $(\tilde{x}_{\text{scat}},\tilde{y}_{\text{scat}},\tilde{z}_{\text{scat}})$ that is reached by the source ray at time t_s and connects to the receiver by the receiver ray taking as initial time t_s. Following the propagation of singularities in $\tilde{D}$, the "horizontal" sunken source coordinates satisfy

$$\tilde{x}_{\text{scat}}-(\tilde{x}-\tilde{h}_x)=\int_{t'_s}^{t_s} dt\,\tilde{v}_{s,x}(t),\quad \tilde{y}_{\text{scat}}-(\tilde{y}-\tilde{h}_y)=\int_{t'_s}^{t_s} dt\,\tilde{v}_{s,y}(t); \tag{4.19}$$

the "horizontal" sunken receiver coordinates satisfy

$$-\tilde{x}_{\text{scat}}+(\tilde{x}+\tilde{h}_x)=\int_{t''_s}^{t_s} dt\,\tilde{v}_{r,x}(t),\quad -\tilde{y}_{\text{scat}}+(\tilde{y}+\tilde{h}_y)=\int_{t''_s}^{t_s} dt\,\tilde{v}_{r,y}(t). \tag{4.20}$$

Adding up these equations results in

$$2\tilde{h}_x = \int_{t'_s}^{t''_s} dt\, \tilde{v}_x(t), \quad 2\tilde{h}_y = \int_{t'_s}^{t''_s} dt\, \tilde{v}_y(t), \tag{4.21}$$

where $(\tilde{v}_x(t), \tilde{v}_y(t))$ is taken from the source ray for $t < t_s$ and from the receiver ray for $t > t_s$.

We introduce a tensor $B_{\sigma\sigma'}$ that is assumed to satisfy the "bound" (cf. (4.18))

$$w^\sigma B_{\sigma\sigma'} w^{\sigma'} \leq w^\sigma c^{-2} \tilde{g}_{\sigma\sigma'} w^{\sigma'}. \tag{4.22}$$

Using the particular structure of the metric tensor, we obtain the estimate

$$2\,(\tilde{h}^\sigma B_{\sigma\sigma'} \tilde{h}^{\sigma'})^{1/2} \leq \int_{t'_s}^{t''_s} \left(\tilde{v}^\sigma c^{-2} \tilde{g}_{\sigma\sigma'} \tilde{v}^{\sigma'}\right)^{1/2} dt \leq |t'_s - t''_s| = |T|, \tag{4.23}$$

which replaces equation 4.7. We conclude that the energy in $\tilde{D}$ is located within the cone in $(\tilde{h}_x, \tilde{h}_y, T)$ space defined by this equation.

The angle transform is an integral of $\tilde{D}$ over a plane in $(\tilde{h}_x, \tilde{h}_y, T)$ space given by $T = \tilde{p}_\sigma \tilde{h}^\sigma$. Let $B^{\sigma\sigma'}$ denote the elements of the inverse of the matrix $B_{\sigma\sigma'}$. Suppose that

$$\tilde{p}_\sigma B^{\sigma\sigma'} \tilde{p}_{\sigma'} < 2, \tag{4.24}$$

which replaces equation 4.9. With

$$|\tilde{p}_\sigma \tilde{h}^\sigma| \leq (\tilde{p}_\sigma B^{\sigma\sigma'} \tilde{p}_{\sigma'})^{1/2} (\tilde{h}^\sigma B_{\sigma\sigma'} \tilde{h}^{\sigma'})^{1/2} \tag{4.25}$$

it then follows that

$$|T| = |\tilde{p}_\sigma \tilde{h}^\sigma| < 2(\tilde{h}^\sigma B_{\sigma\sigma'} \tilde{h}^{\sigma'})^{1/2}, \tag{4.26}$$

which replaces equation 4.10. Using the same arguments as before, it follows, again, that the energy in the angle transform is located only at the true scattering point independent of $\tilde{p}$. This also implies that annihilators of the data can be constructed from

$$\frac{\partial}{\partial(\tilde{p}_x, \tilde{p}_y)} \int dS(\tilde{h}_x, \tilde{h}_y) \left(\frac{\partial}{\partial t}\right)^{-1} \tilde{D}(\tilde{x}, \tilde{y}, \tilde{z}, \tilde{h}_x, \tilde{h}_y, \tilde{p}_\sigma \tilde{h}^\sigma)\, \chi(\tilde{h}_x, \tilde{h}_y),$$

cf. equation 4.17; these annihilators drive wave-equation migration velocity analysis in the presence of caustics and turning rays.

5. Example. We illustrate the semblance property established in the preceding pages for shot-geophone migration. In an example, containing a low velocity lens, we expose the dramatic contrast between image (or common-image-point) gathers produced by shot-geophone migration and those produced by other forms of prestack depth migration. The formation of caustics leads to failure of the semblance principle for Kirchhoff (or Generalized Radon Transform) common scattering angle migration. The DSR assumption is satisfied for the acquisition offsets considered. For the shot-geophone migration we employ a method based on solving Helmholtz equations [29]. We form angle image gathers by Radon transform in offset and time, following [10].

The example was used in [34, 33] to show that common offset and Kirchhoff (or generalized Radon transform) common scattering-angle migration produce strong kinematic artifacts in strongly refracting velocity models. The velocity model (Figure 7) consists of a slow Gaussian lens embedded in a constant background. This model is strongly refracting through the formation of triplications in the rayfields. Below the lens, at a depth of 2 km, we placed a flat, horizontal reflector. We synthesized data using a $(4, 10, 20, 40)$ Hz zero phase bandpass filter as (isotropic) source wavelet, and a finite difference scheme with adequate sampling. A typical shot gather over the lens (Figure 8, shot position indicated by a vertical arrow in Figure 7) shows a complex pattern of reflections from the flat reflector that have propagated through the lens.

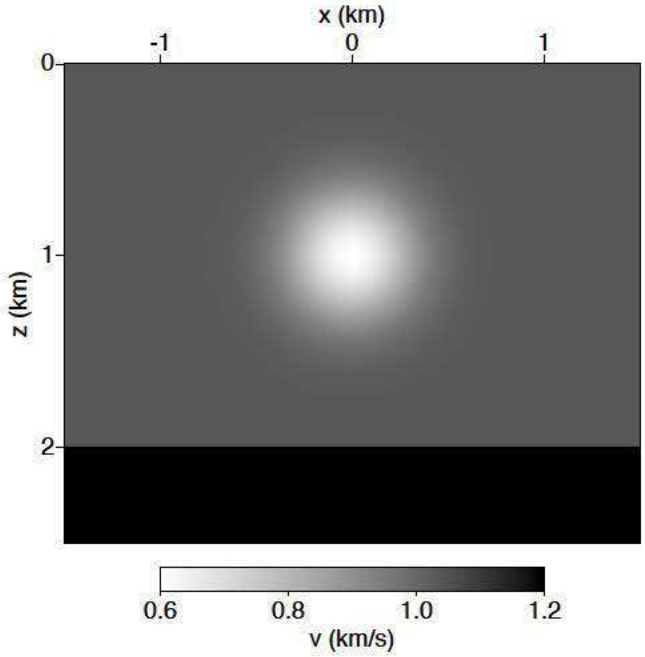

FIGURE 7. *Lens velocity model over flat reflector.*

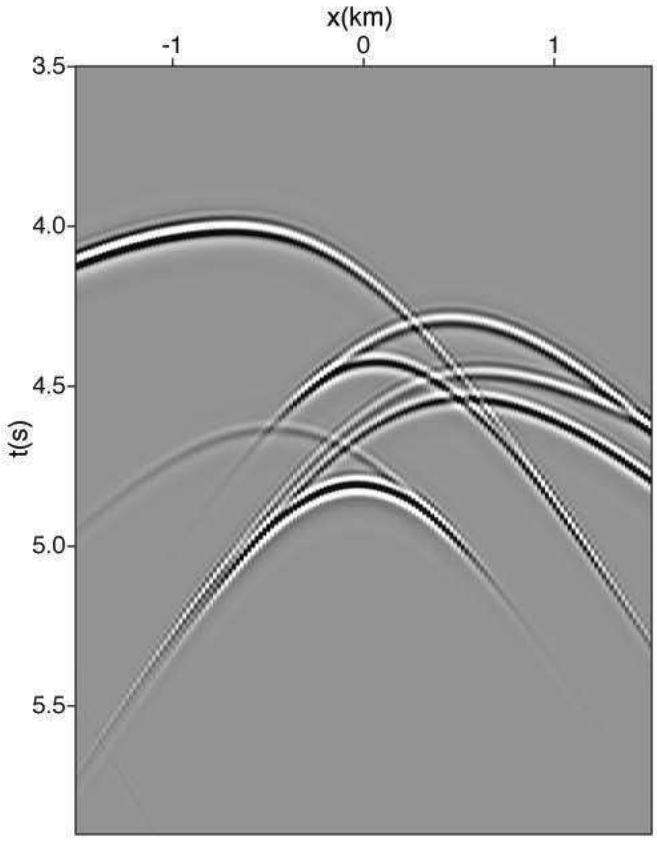

FIGURE 8. *Lens model, shot record at shot location* -500 *m.*

We migrated the data with the above mentioned approach. Figure 9 shows the image, which clearly reproduces the reflector. An angle image gather is shown in Figure 10 for comparison we show the Kirchhoff common scattering angle image gather in Figure 11 at the same location (left) reproduced from [33], each trace of which is obtained by Kirchhoff migration restricted to common angle. The Kirchhoff image gather is clearly contaminated by numerous energetic non-flat events, while the wave equation image gather is not. Artifacts in the Kirchhoff image gather must be non flat and can be removed by "dip" filtering in depth and angle or isochron filtering, but only if the velocity model is perfectly well known.

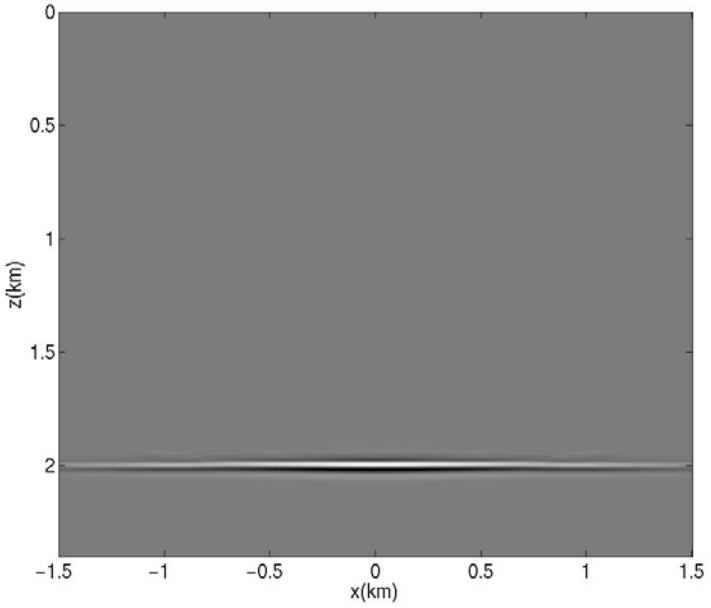

FIGURE 9. *Wave-equation image of data lens velocity model, flat reflector.*

6. Conclusion. We have demonstrated, mathematically and by example, that shot-geophone migration produces artifact-free image volumes, assuming (i) a kinematically correct and relatively smooth velocity model, (ii) a (local) curvilinear coordinate system and an associated Riemannian metric admitting the introduction of pseudodepth with respect to which incident energy travels "downwards" and reflected energy travels "upwards", and (iii) enough data to uniquely determine rays corresponding to events in the data. In an example, we compared shot-geophone migration with Kirchhoff common scattering angle migration. While the latter technique bins data only implicitly, it is like other binwise migration schemes, such as common offset migration, in generating kinematic image artifacts in prestack data when the velocity model is sufficiently complex to strongly refract waves.

The literature contains a number of comparisons of Kirchhoff and wave equation migration (for example, [1, 15]). Performance differences identified in these reports have been ascribed to a wide variety of factors, such as differences in anti-aliasing and decimation strategies, choice of time fields used in Kirchhoff imaging, and "fidelity" to the wave equation. These factors surely affect performance, but reflect mainly implementation decisions. The difference identified and demonstrated in this paper, on the other hand, is *fundamental*: it flows from the differing formulations of prestack imaging (and modeling) underlying the two classes of methods. No implementation variations can mask it.

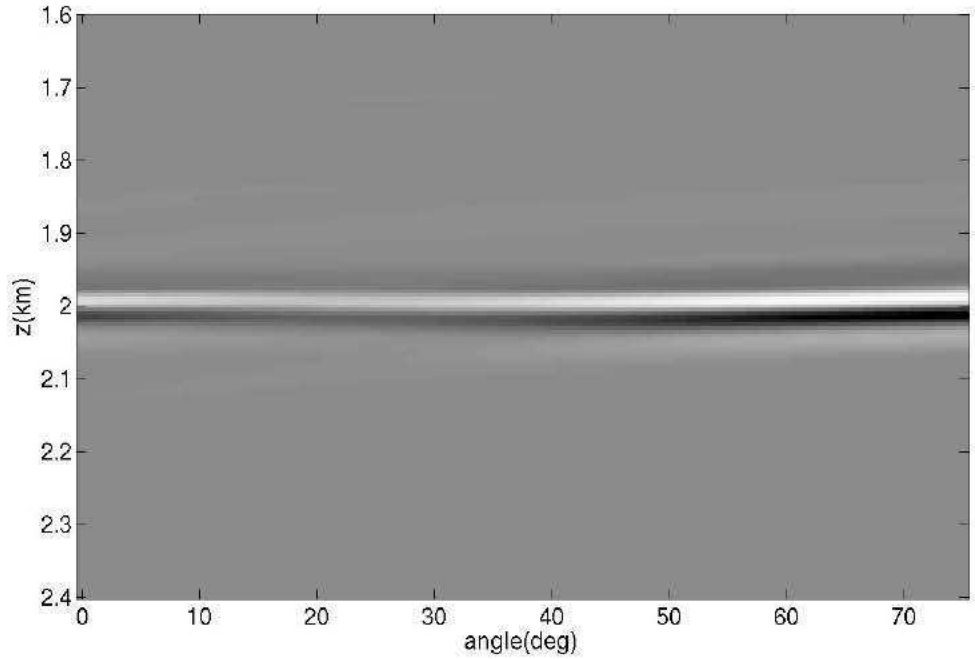

FIGURE 10. *Lens model, common image point gather obtained with the wave-equation angle transform at* $x_m = 300\ m$.

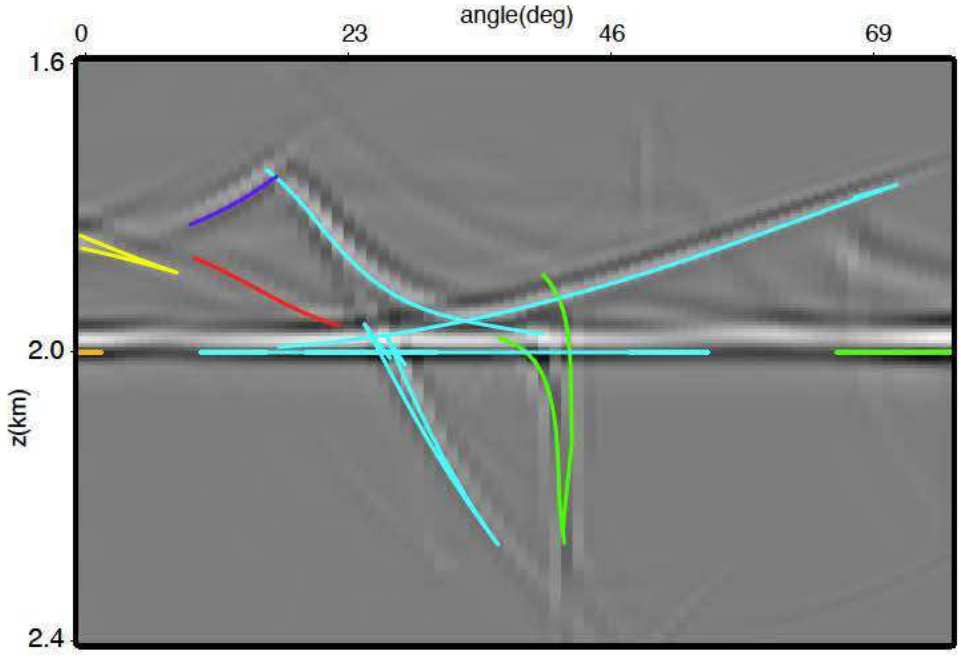

FIGURE 11. *Lens model, common image point gather obtained with the Kirchhoff angle transform at* $x_m = 300\ m$.

In fact, we have shown that implementation has at most a secondary impact on kinematic accuracy of shot-geophone imaging. Its basic kinematics is shared not just by the two common depth extrapolation implementations - shot profile, double square root - but also by a variant of reverse time imaging and even by a Kirchhoff or Generalized Radon Transform operator of appropriate construction. Naturally these various options differ in numerous ways, in their demands on data quality and sampling and in their sensitivity to various types of numerical artifacts. However in the ideal limit of continuous data and discretization-free computation, all share an underlying kinematic structure and offer the potential of artifact-free data volumes when the assumptions of our theory are satisfied, even in the presence of strong refraction and multiple arrivals at reflecting horizons.

It remains to address three shortcomings of the theory. The first is its reliance on a (local) curvilinear coordinate system and corresponding "DSR" assumption. This restricts the class of allowable "turning rays" (but reflections off a vertical salt flank, where pseudodepth becomes close to horizontal, can satisfy this assumption). Indeed, numerical investigations of Biondi and Shan [5] suggested that reverse time (two-way) wave equation migration, as presented here, could be modified by inclusion of nonhorizontal offsets to permit the use of turning energy, and indeed to image reflectors of arbitrary dip. This latter possibility has been understood in the context of (stacked) images for some time [39]. Biondi and Shan [5] present prestack image gathers for horizontal and vertical offsets which suggested that a similar flexibility may be available for the shot-geophone extension. Biondi and Symes [6] give a local analysis of shot-geophone image formation using nonhorizontal offsets, whereas Symes [35] studied globally the formation of kinematic artifacts in a horizontal / vertical offset image volume. Such artifacts cannot be entirely ruled out; however, kinematic artifacts cannot occur at arbitrarily small offset, in contrast to the formation of artifacts at all offsets in binwise migration.

A second limitation of our main result is its assumption that ray kinematics are completely determined by the data. Of course this is no limitation for the 2D synthetic examples presented above. With the advent of WATS acquisition this limitation is overcome as well. However most contemporary data are acquired with narrow-azimuth streamer equipment. For such data, we cannot in general rule out the appearance of artifacts due to multiple ray pairs satisfying the shot-geophone kinematic imaging conditions. However two observations suggest that all is not lost in this situation. First, for ideal "2.5D" structure (independent of crossline coordinate) and perfect linear survey geometry (no feathering), all energetic rays remain in the vertical planes through the sail line, and our analysis applies without alteration to guarantee imaging fidelity. Second, the conditions that ensure absence of artifacts are *open*, i.e. small perturbations of velocity and source and receiver locations cannot affect the conclusion. Therefore shot-geophone imaging fidelity is robust against mild crossline heterogeneity and small amounts of cable feathering. Note that nothing about the *formulation* of our modeling or (adjoint) migration operators requires areal geometry - the operators are perfectly well-defined for narrow azimuth data.

An intriguing and so far theoretically untouched area concerns the potential of *multiple* narrow azimuth surveys, with distinct central azimuths, to resolve the ambiguities of single azimuth imaging.

A third, and much more fundamental, limitation pertains to migration itself. Migration operators are essentially adjoints to *linearized* modeling operators. The kinematic theory of migration requires that the velocity model be slowly varying on the wavelength scale, or at best be slowly varying except for a discrete set of fixed, regular interfaces. The most challenging contemporary imaging problems, for example subsalt prospect assessment, transgress this limitation, in many cases violently. Salt-sediment interfaces are amongst the unknowns, especially bottom salt, are quite irregular, and are perhaps not even truly interfaces. Very clever solutions have been and are being devised for these difficult imaging problems, but the theory lags far, far behind the practice.

7. Acknowledgements. This work was supported in part by the National Science Foundation, and by the sponsors of The Rice Inversion Project (TRIP). MdH also acknowledges support by the members of the Geo-Mathematical Imaging Group (GMIG). CS acknowledges support from the Netherlands Organization for Scientific Research NWO under grant no. 639.032.509. We thank

Shen Wang for his help in generating the examples, and Norman Bleistein for careful scrutiny of an early draft.

8. Appendix. In this appendix we establish the relation between the appearance of events in the data and the presence of reflectors in the migrated image. This relation is the *same* for the forward modeling operator and for its adjoint, the migration operator.

The reasoning presented here shares with [30] the identification of events, respectively reflectors, by high frequency asymptotics in phase space, but differs in that it does not explicitly use oscillatory integral representations of $F[v]$. Instead, this argument follows the pattern of Rakesh's analysis of shot profile migration kinematics [23]. It can be made mathematically rigorous, by means of the so-called Gabor calculus in the harmonic analysis of singularities (see [14] Ch. 1).

Our analysis is based on the recognition that the shot-geophone predicted data field $u(\mathbf{x}_r, t; \mathbf{x}_s)$, defined by equation 2.10, is the value at $\bar{\mathbf{x}} = \mathbf{x}_r$ of the space-time field $u(\bar{\mathbf{x}}, t; \mathbf{x}_s)$, which solves

$$\frac{1}{v^2(\bar{\mathbf{x}})}\frac{\partial^2 u}{\partial t^2}(\bar{\mathbf{x}}, t; \mathbf{x}_s) - \nabla^2_{\bar{\mathbf{x}}} u(\bar{\mathbf{x}}, t; \mathbf{x}_s) = \int d\mathbf{h}\, R(\bar{\mathbf{x}} - \mathbf{h}, \mathbf{h})\frac{\partial^2}{\partial t^2} G(\bar{\mathbf{x}} - 2\mathbf{h}, t; \mathbf{x}_s) \tag{A-1}$$

This equation follows directly by applying the wave operator to both sides of equation 2.10.

The appearance of an event at a point $(\mathbf{x}_s, \mathbf{x}_r, t_{sr})$ in the data volume is equivalent to the presence of a sizeable Fourier coefficient for a plane wave component

$$e^{i\omega(t - \mathbf{p}_s\cdot\bar{\mathbf{x}}_s - \mathbf{p}_r\cdot\bar{\mathbf{x}}_r)} \tag{A-2}$$

in the acoustic field for frequencies ω within the bandwidth of the data, even after muting out all events at a small distance from $(\mathbf{x}_s, \mathbf{x}_r, t_{sr})$.

Note that the data does not necessarily fully determine this plane wave component, i.e. the full 3D event slownesses $\mathbf{p}_s, \mathbf{p}_r$. In this appendix, $\mathbf{p}_s, \mathbf{p}_r$ are assumed to be compatible with the data, in the sense just explained.

Assume that these frequencies are high enough relative to the length scales in the velocity that such local plane wave components propagate according to geometric acoustics. This assumption tacitly underlies much of reflection processing, and in particular is vital to the success of migration.

That is, solutions of wave equations such as A-1 carry energy in local plane wave components along rays. Let $(\mathbf{X}_r(t), \mathbf{P}_r(t))$ denote such a ray, so that $\mathbf{X}_r(t_{sr}) = \mathbf{x}_r, \mathbf{P}_r(t_{sr}) = \mathbf{p}_r$. Then at some point the ray must pass through a point in phase space at which the source term (right hand side) of equation A-1 has significant energy - otherwise the ray would never pick up any energy at all, and there would be no event at time t_{sr}, receiver position $\mathbf{x}_r$, and receiver slowness $\mathbf{p}_r$. [Supplemented with proper mathematical boilerplate, this statement is the celebrated *Propagation of Singularities* theorem of Hörmander, [17, 36].]

The source term involves (i) a product, and (ii) an integral in some of the variables. The Green's function $G(\bar{\mathbf{x}}_s, t, \mathbf{x}_s)$ has high frequency components along rays from the source, i.e. at points of the form $(\mathbf{X}_s(t_s), \mathbf{P}_s(t_s))$ where $\mathbf{X}_s(0) = \mathbf{x}_s$ and $t_s \geq 0$. [Of course this is just another instance of Propagation of Singularities, as the source term in the wave equation for $G(\bar{\mathbf{x}}_s, t_s, \mathbf{x}_s)$ is singular only at $(\mathbf{x}_s, 0)$.] That is, viewed as a function of $\bar{\mathbf{x}}_s$ and t_s, $G(\cdot, \cdot; \mathbf{x}_s)$ will have significant Fourier coefficients for plane waves

$$e^{i\omega(\mathbf{P}_s(t_s)\cdot\bar{\mathbf{x}}_s + t_s)} \tag{A-3}$$

We characterize *reflectors* in the same way: that is, there is a (double) reflector at $(\bar{\mathbf{x}}_s, \bar{\mathbf{x}}_r)$ if $\bar{R}$ has significant Fourier coefficients of a plane wave

$$e^{i(\mathbf{k}_s\cdot\bar{\mathbf{x}}'_s + \mathbf{k}_r\cdot\bar{\mathbf{x}}'_r)} \tag{A-4}$$

for some pair of wavenumbers $\mathbf{k}_s, \mathbf{k}_r$, and for generic points $(\bar{\mathbf{x}}'_s, \bar{\mathbf{x}}'_r)$ near $(\bar{\mathbf{x}}_s, \bar{\mathbf{x}}_r)$. Presumably then the product $R(\bar{\mathbf{x}}'_s, \mathbf{x})G(\bar{\mathbf{x}}'_s, t_s; \mathbf{x}_s)$ has a significant coefficient of the plane wave component

$$e^{i((\mathbf{k}_s + \omega\mathbf{P}_s(t_s))\cdot\bar{\mathbf{x}}'_s + \mathbf{k}_r\cdot\mathbf{x} + \omega t_s)} \tag{A-5}$$

for $\bar{\mathbf{x}}_s'$ near $\bar{\mathbf{x}}_s$, $\mathbf{x}$ near $\bar{\mathbf{x}}_r$; note that implicitly we have assumed that $\bar{\mathbf{x}}_s$ (the argument of G) is located on a ray from the source with time t_s. The right-hand side of equation A-1 integrates this product over $\bar{\mathbf{x}}_s$. This integral will be negligible unless the phase in $\bar{\mathbf{x}}_s$ is stationary: that is, to produce a substantial contribution to the RHS of equation A-1, it is necessary that

$$\bar{\mathbf{x}}_s = \mathbf{X}_s(t_s),\ \mathbf{k}_s + \omega \mathbf{P}_s(t_s) = 0 \tag{A-6}$$

Supposing that this is so, the remaining exponential suggests that the RHS of equation A-1 has a sizeable passband component of the form

$$e^{i(\mathbf{k}_r \cdot \mathbf{x} + \omega t_s)} \tag{A-7}$$

for $\mathbf{x}$ near $\bar{\mathbf{x}}_r$. As was argued above, this RHS will give rise to a significant plane wave component in the solution u arriving at $\mathbf{x}_r$ at time $t_{sr} = t_s + t_r$ exactly when a ray arriving at $\mathbf{x}_r$ at time t_{sr} starts from a position in space-time with the location and wavenumber of this plane wave, at time $t_s = t_{sr} - t_r$: that is,

$$\mathbf{X}_r(t_s) = \bar{\mathbf{x}}_r,\ \omega \mathbf{P}_r(t_s) = \mathbf{k}_r \tag{A-8}$$

We end this appendix with a remark about the case of *complete coverage*, i.e. sources and receivers densely sample a fully 2D area on or near the surface. Assuming that the effect of the free surface has been removed, so that all events may be viewed as samplings of an upcoming wavefield, the data (2D) event slowness uniquely determines the wavefield (3D) slowness through the eikonal equation. Thus an event in the data is characterized by its (3D) moveout: locally, by a moveout equation $t = T(\mathbf{x}_s, \mathbf{x}_r)$, and infinitesimally by the source and receiver slownesses

$$\mathbf{p}_s = \nabla_{\mathbf{x}_s} T,\ \mathbf{p}_r = \nabla_{\mathbf{x}_r} T \tag{A-9}$$

In this case, the data event uniquely determines the source and receiver rays.

REFERENCES

[1] Albertin, U., Watts, D., Chang, W., Kapoor, S. J., Stork, C., Kitchenside, P., and Yingst, D., 2002, Near-salt-flank imaging with kirchhoff and wavefield-extrapolation migration: 72nd Annual International Meeting, Society of Exploration Geophysicists, Expanded Abstracts, 1328–1331.

[2] Albertin, U., Sava, P. C., Etgen, J., and Maharramov, M., 2006, Adjoint wave-equation velocity analysis: 76th Annual International Meeting, Society of Exploration Geophysicists, Expanded Abstracts.

[3] Barley, B., and Summers, T., 2007, Multi-azimuth and wide-azimuth seismic: Shallow to deep water, exploration to production: The Leading Edge, **26**, 450–457.

[4] Biondi, B., 2003, Equivalence of source-receiver migration and shot-profile migration: Geophysics, **68**, 1340–1347.

[5] Biondi, B., and Shan, G., 2002, Prestack imaging of overturned reflections by reverse time migration: 72nd Annual International Meeting, Society of Exploration Geophysicists, Expanded Abstracts, 1284–1287.

[6] Biondi, B., and Symes, W., 2004, Angle-domain common-image gathers for migration velocity analysis by wavefield-continuation imaging: Geophysics, **69**, 1283–1298.

[7] Brandsberg-Dahl, S., De Hoop, M. V., and Ursin, B., 2003, Focusing in dip and AVA compensation on scattering angle/azimuth common image gathers: Geophysics, **68**, 232–254.

[8] Claerbout, J. F., 1971, Toward a unified theory of reflector mapping: Geophysics, **36**, 467–481.

[9] Claerbout, J., 1985, Imaging the earth's interior: Blackwell Scientific Publishers, Oxford.

[10] De Bruin, C. G. M., Wapenaar, C. P. A., and Berkhout, A. J., 1990, Angle-dependent reflectivity by means of prestack migration: Geophysics, **55**, 1223–1234.

[11] De Hoop, M. V., and Bleistein, N., 1997, Generalized Radon transform inversions for reflectivity in anisotropic elastic media: Inverse Problems, **13**, 669–690.

[12] De Hoop, M. V., Le Rousseau, J., and Biondi, B., 2003, Symplectic structure of wave-equation imaging: A path-integral approach based on the double-square-root equation: Geoph. J. Int., **153**, 52–74.

[13] De Hoop, M. V., Van der Hilst, R.D. and Shen, P., 2006, Wave-equation reflection tomography: Annihilators and sensitivity kernels: Geoph. J. Int., **167**, 1332–1352.

[14] Duistermaat, J. J., Fourier integral operators: Lecture notes, Courant Institute, New York, 1973.

[15] Fliedner, M. M., Crawley, S., Bevc, D., Popovici, A. M., and Biondi, B., 2002, Imaging of a rugose salt body in the deep gulf of mexico: Kirchhoff versus common azimuth wave-equation migration: 72nd Annual International Meeting, Society of Exploration Geophysicists, Expanded Abstracts, 1304–1307.

[16] Friedlander, F. G., The wave equation on a curved space-time, Cambridge University Press, Cambridge, 1976.
[17] Hörmander, L., 1983, The analysis of linear partial differential operators: Volume I, Springer Verlag, Berlin.
[18] Kleyn, A., 1983, Seismic reflection interpretation: Applied Science Publishers, New York.
[19] Michell, S., Shoshitaishvili, E., Chergotis, D., Sharp, J., and Etgen, J., Wide azimuth streamer imaging of Mad Dog: H ave we solved the subsalt imaging problem?: 76th Annual International Meeting, Society of Exploration Geophysicists, Expanded Abstracts, 2905–2909.
[20] Nolan, C. J., and Symes, W. W., 1996, Imaging and conherency in complex structure: 66th Annual International Meeting, Society of Exploration Geophysicists, Expanded Abstracts, 359–363.
[21] Nolan, C., and Symes, W., 1997, Global solution of a linearized inverse problem for the wave equation: Comm. P.D.E., **22**, 919–952.
[22] Prucha, M., Biondi, B., and Symes, W., 1999, Angle-domain common image gathers by wave-equation migration: 69th Annual International Meeting, Society of Exploration Geophysicists, Expanded Abstracts, 824–827.
[23] Rakesh, 1988, A linearized inverse problem for the wave equation: Comm. on P.D.E., **13**, no. 5, 573–601.
[24] Sava, P., and Biondi, B., 2004, Wave-equation migration velocity analysis – I: Theory: Geophys. Prosp., **52**, 593–606.
[25] Sava, P., and Fomel, S., 2003, Angle-domain common-image gathers by wavefield continuation methods: Geophysics, **68**, 1065–1074.
[26] Sava, P., and Fomel, S., 2005, Riemannian wavefield extrapolation: Geophysics, **70**, T45–T56.
[27] Schultz, P., and Sherwood, J., 1982, Depth migration before stack: Geophysics, **45**, 376–393.
[28] Shen, P., Symes, W., and Stolk, C. C., 2003, Differential semblance velocity analysis by wave-equation migration: 73rd Annual International Meeting, Society of Exploration Geophysicists, Expanded Abstracts, 2135–2139.
[29] Sirgue, L., and Pratt, R. G., Efficient waveform inversion and imaging: A strategy for selecting temporal frequencies: Geophysics, **69**, 231–248.
[30] Stolk, C. C., and De Hoop, M. V., December 2001, Seismic inverse scattering in the 'wave-equation' approach, Preprint 2001-047, The Mathematical Sciences Research Institute, http://msri.org/publications/preprints/2001.html.
[31] Stolk, C. C., and De Hoop, M. V., Modeling of seismic data in the downward continuation approach: SIAM J. Appl. Math., **65**, 1388–1406,
[32] Stolk, C. C., and De Hoop, M. V., Seismic inverse scattering in the downward continuation approach: Wave Motion, **43**, 579–598.
[33] Stolk, C. C., and Symes, W. W., 2004, Kinematic artifacts in prestack depth migration: Geophysics, **69**, 562–575.
[34] Stolk, C. C., 2002, Microlocal analysis of the scattering angle transform: Comm. P. D. E., **27**, 1879–1900.
[35] Symes, W. W., 2002, Kinematics of reverse time shot-geophone migration, The Rice Inversion Project, Department of Computational and Applied Mathematics, Rice University, Houston, Texas, USA: http://www.trip.caam.rice.edu.
[36] Taylor, M., 1981, Pseudodifferential operators: Princeton University Press, Princeton, New Jersey.
[37] Xu, S., Chauris, H., Lambaré, G., and Noble, M., 2001, Common angle migration: A strategy for imaging complex media: Geophysics, **66**, no. 6, 1877–1894.
[38] Yilmaz, O., 1987, Seismic data processing: Investigations in Geophysics No. 2.
[39] Yoon, K., Shin, C., Suh, S., Lines, L., and Hong, S., 2003, 3d reverse-time migration using the acoustic wave equation: An experience with the SEG/EAGE data set: The Leading Edge, **22**, 38.